RAPID COMMUNICATION

Interaction between Matrix Cracks in E-Glass/Epoxy Two-Dimensional Multi-Fiber-Array Model Composites

GALE A. HOLMES, WALTER G. MCDONOUGH, JOY P. DUNKERS, CHARLES C. HAN

Polymers Division, Multiphase Materials Group, National Institute of Standards and Technology, Building 224, Room B108, 100 Bureau Drive Stop 8543, Gaithersburg, Maryland 20899

Received 6 March 2002; revised 28 February 2003; accepted 28 February 2003

Keywords: fiber–fiber interactions; failure; optical coherence tomography; composites; fibers; fracture; thermosets

The failure of composites has been the subject of intense research for many years.[1–3] Although there are several composite failure mechanisms (e.g., fiber fracture, matrix cracking, delamination, and fiber-matrix debonding), the interphase region between the fiber and the matrix has been a critical factor in all of these failure modes. This observation has fueled sustained and continuous research focus during the past 40 years on fiber-matrix interface strength. Although significant information has been obtained about the interphase region and its impact on composite failure, experimental micromechanics research to assess the influence of this parameter on the initiation and propagation of the different composite failure modes is a recent endeavor.

In this communication, fragmentation data are presented for two-dimensional (2D) multi-fiber-array composites containing E-glass fibers that fracture with associated fiber-matrix debonding and matrix crack formation. Research on 2D multi-fiber-array composites had its genesis in the 1989 experimental research of Wagner and Steenbakkers[4] in which they devised a methodology for constructing these arrays with controlled fiber spacing. From a micromechanics perspective, the experimental approach developed by Wagner and Steenbakkers[4] provides a means of probing the interaction between fibers during fiber fracture and yields an approach for assessing the validity of computational models used to predict composite failure behavior. Computationally, chain-of-bundles models, for example, Phoenix and Beyerlein[5] or Hedgepeth and van Dyke,[6] provide the framework for predicting the strength and failure behavior of uniaxial composites with the experimental data from these 2D multifiber arrays.

Most of this multifiber research has focused on laser Raman spectroscopy (LRS) as a detection tool for directly measuring the strain in broken and unbroken fibers.[7–19] In particular, the magnitude and location of the overstressed region in the fibers adjacent to the broken fibers has been cited as a critical fiber–fiber-interaction effect that controls the initial composite failure process (see Fig. 1). Until recently, this technique was restricted to Raman-active fibers. In 2000, Young's research group[20,21] succeeded in monitoring the fracture of 100 μm glass fibers by coating the surface with a Raman-active polymer before embedding the fiber in a flexible epoxy matrix. Wood and coworkers[22–25] recently suggested with single-wall carbon nanotubes probing the mechanical properties of the matrix and obtaining information about the fracture of glass fibers.

Even with these potential approaches, the applicability of the LRS results to glass fiber composites is now restricted because the use of adhesion promoters on glass fibers increases the interphase strength and often introduces matrix crack formation as a failure mode that accompanies fiber-matrix debonding during fiber fracture. In addition, most of this multifiber research has focused on the failure of these Raman-active fibers

Correspondence to: G. A. Holmes (E-mail: gale.holmes@nist.gov)

Journal of Polymer Science: Part B: Polymer Physics, Vol. 41, 2976–2981 (2003)

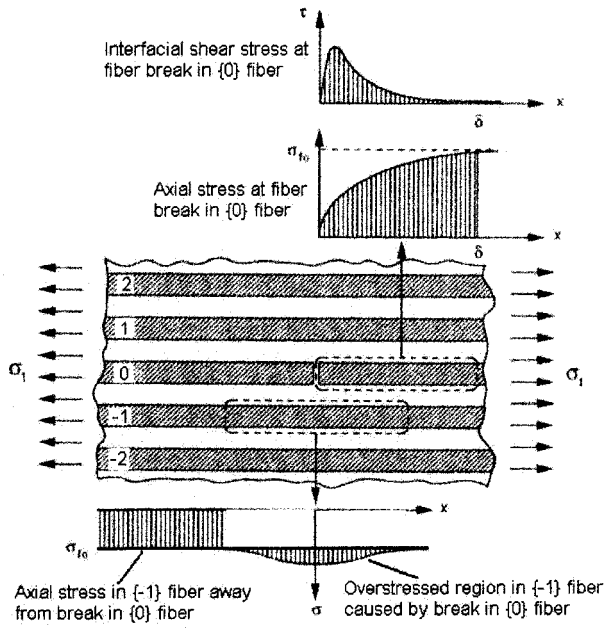

Figure 1. Local stress distributions around a fiber break in a 2D multi-fiber-array model composite under longitudinal tension. Fiber numbers (left side of array) conform to the designation of Sastry and Phoenix (refs. 26 and 27). In the text, {} brackets surround the fiber number in the array (figure adapted from ref. 28).

in low- or room temperature-cured resins [e.g., diglycidyl ether of bisphenol A (DGEBA) cured with polyetheramine (Jeffamine T-403)[8] or UV-curable urethane diacrylate oligomer and benzyl ketal photoinitiator[12]]. Translating these results to high-temperature epoxy resins, which are often used in structural composites, is problematic because the yield behavior, failure strains, failure behavior of the fiber-matrix interphase, cure kinetics, and residual cure stresses in these materials are different.

To develop a fundamental understanding of glass-fiber composite failure mechanisms with model composites, control of the fiber-matrix interphase, with a well-characterized and industrially relevant matrix, is desirable. For the matrix, an epoxy resin formulated by Drzal and Herera-Franco[29] is used. The formulation consists of stoichiometric proportions of DGEBA and *meta*-phenylenediamine (*m*-PDA) that is undercured with the following curing profile to increase the matrix ductility while maintaining a high glass-transition temperature: 2 h at 75 °C followed by 2 h at 125 °C. Analogous systems are used industrially in the preparation of composites by filament winding. Therefore, studies with this model epoxy resin are relevant to industrial processes.

With respect to the fiber-matrix interphase, E-glass fibers coated with a self-assembled monolayer (SAM) of 11-aminoundecane trichlorosilane (11-AUTCS) have been investigated. SAM interfaces can potentially reduce the complexity of the fiber-matrix interphase region and provide an approach for separating the effects of covalent bonding, mechanical interlocking, and physicochemical forces on interphase adhesion. In addition, the failure behavior associated with fiber fracture can be investigated by controlling the degree of bonding sites on the fiber surface. As an example, previous research[30] with DGEBA/*m*-PDA epoxy resin has demonstrated that when a SAM-coated E-glass fiber fractures, fiber-matrix interphase debonding is accompanied by matrix crack formation. This failure behavior is identical to that found in E-glass fibers coated industrially with γ-aminopropyltrialkoxy silanes. In contrast to this behavior, research in the National Institute of Standards and Technology laboratory has suggested that the interphase strength of a bare E-glass fiber embedded in the DGEBA/*m*-PDA epoxy resin is compa-

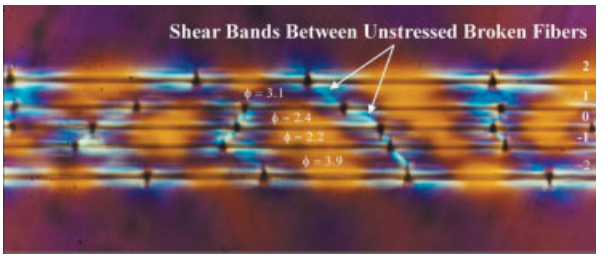

Figure 2. Optical micrograph with crossed polarizers of fiber break (seen as dark holes in fibers) patterns from E-glass/DGEBA/*m*-PDA 2D multifiber array immediately after removing stress. The interfiber spacing is denoted by ϕ. Fiber numbers (right side of figure) conform to the designation of Sastry and Phoenix (refs. 26 and 27). [Color figure can be viewed in the online issue, which is available at www.interscience.wiley.com]

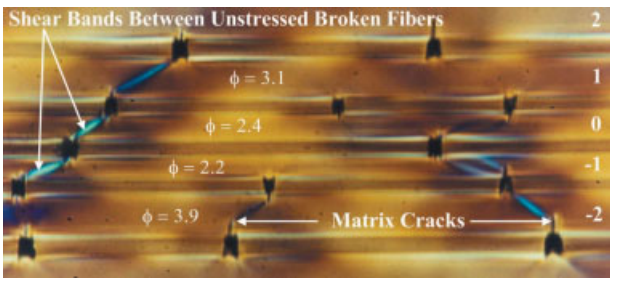

Figure 3. Optical micrograph with crossed polarizers of fiber break (dark regions in fibers) patterns from E-glass/DGEBA/*m*-PDA 2D multifiber array 24 h after removing stress. The interfiber spacing is denoted by ϕ. Fiber numbers (right side of figure) conform to the designation of Sastry and Phoenix (refs. 26 and 27). [Color figure can be viewed in the online issue, which is available at www.interscience.wiley.com]

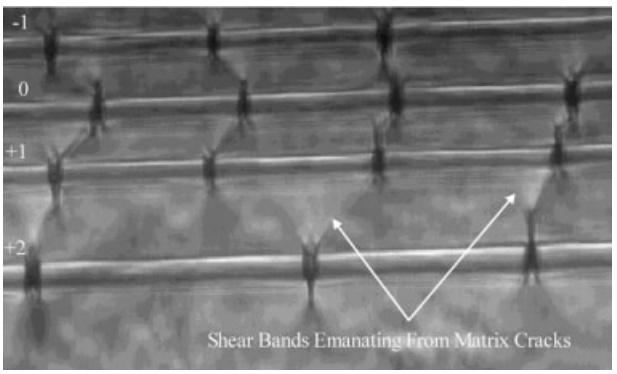

Figure 4. Optical micrograph of fiber break (dark regions in fibers) patterns from E-glass/DGEBA/*m*-PDA 2D multifiber array (stressed). The interfiber spacing is denoted by ϕ. Fiber numbers (left side of figure) conform to the designation of Sastry and Phoenix (refs. 26 and 27). The {2} fiber is not shown.

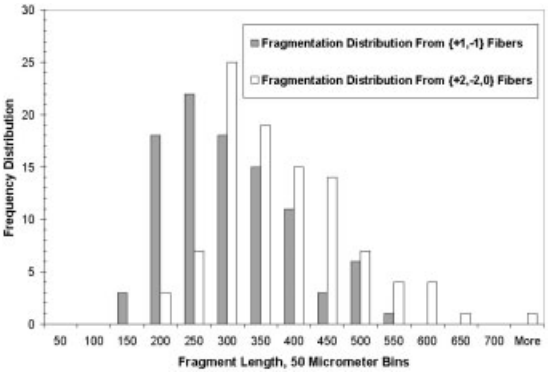

Figure 6. Aggregated histograms comparing fragment distributions of {±2,0} fibers with {±1} fibers in E-glass/DGEBA/*m*-PDA 2D multifiber array. E-glass fibers coated with 11-AUTCS.

rable to that of the silane interphases but fails primarily by fiber-matrix debonding. These results suggest that the intrinsic toughness of the interphase region and/or the nature of the bonding in this region controls the initial failure modes of the composite.

In this research, fiber fracture data are presented on 2D multi-fiber-array model composites where the E-glass fiber is coated with 11-AUTCS and embedded in DGEBA/*m*-PDA epoxy resin.[31] The fracture patterns generated by a 2D five-fiber-array model composite are depicted in Figures 2 and 3. Consistent with previous research, the fibers are labeled on the right- or left-hand side of the figures with the central fiber having the "0" designation. The {} brackets are used when identifying fibers in the 2D array. The "±" symbol is used inside the {} brackets when a pair of fibers is being designated. For example, the {±2} designation denotes the {2} fiber and the {−2} fiber that are at the top and bottom, respectively, in Figures 2 and 3.

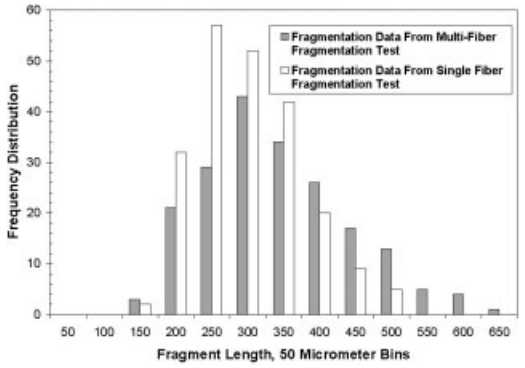

Figure 5. Aggregated histograms of fragmentation data from single-fiber and multi-fiber-fragmentation tests. Test specimens consisted of E-glass fibers coated with 11-AUTCS and embedded in DGEBA/*m*-PDA epoxy resin.

The spacing between fibers, ϕ, is given in each figure in terms of the actual distance divided by 14 μm, which is the nominal fiber diameter of the {±1 and 0} fibers. In all other instances, the "±" symbol is also used to denote one standard deviation about a mean.

In the fracture patterns portrayed in Figures 2 and 3, all fiber breaks are nonaligned (not vertically aligned) although the fibers are spaced two to four fiber diameters apart. These staggered breaks are similar to the fracture patterns investigated computationally by Sastry and Phoenix (see Figs. 6 and 9 in ref. 26).

The change in matrix color from Figure 2 to Figure 3 is due to the relaxation of the stress in the viscoelastic epoxy resin matrix. Figure 2 was taken immediately after the relaxation of the applied stress, whereas Figure 3 was taken after approximately 24 h. In these figures, the nonaligned breaks appear to be located approximately 45° from the adjacent break. In connection with these nonaligned breaks, intense shear bands are located in the matrix between the fiber breaks. The intensity of these shear bands persists long after the stress in the bulk matrix relaxes (cf. Figs. 2 and 3). Data taken during the test, where the specimen is under tension, also indicates the existence of these shear bands between the tip of the matrix cracks (see Fig. 4). In an attempt to clearly determine the shear bands emanating from the crack tips, the {2} fiber is not shown in Figure 4.

Now, we speculate that the origin of these shear bands resides in the fact that the matrix cracks are essentially penny-shaped cracks.[32] Penny-shaped cracks subjected to uniaxial tensile loads generate 45° deformation shear bands that form relative to the tensile axis at the crack tip. The deformation bands emanating from the crack tips in Figure 4 may be related to this phenomenon. The influence of these bands on fracture initiation in the adjacent fiber is not known. How-

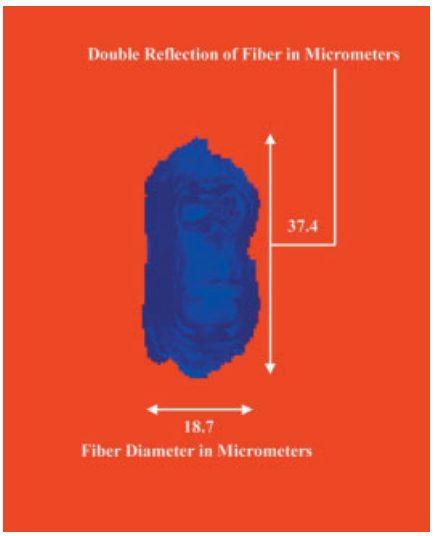

Figure 7. OCT image of a single E-glass fiber (blue) embedded in DGEBA/*m*-PDA matrix (red). Data obtained with optical coherence tomography.

ever, the occurrence of three nonaligned fiber break clusters with identical shapes in the top three fibers in Figure 4 may reflect a deflection of the stress-concentration factor in the adjacent fiber fragments in a manner different from that described by Hedgepeth and van Dyke.[6] Hedgepeth and van Dyke[6] assumed composite failure occurs by a single, perfect transverse line of fiber breaks caused by the increased probability of failure in the region of the adjacent fiber directly across from the initial fiber break (overstress region).

Sastry and Phoenix,[26,27] noting that fiber breaks in real composites are often nonaligned, appear to be the first to connect this nonalignment by theoretical calculations of composite toughness. With a break-influence superposition technique, these researchers concluded that nonaligned fiber breaks could lessen the severity of overload stress concentrations in adjacent fibers or "shield" the fiber break. Sastry and Phoenix[26,27] also concluded that the "shielding" effect is due to the inability of a broken fiber end to bear much tensile load within some axial distance of its broken end and the opposite sign of the shear forces on pairs of broken fiber ends. Therefore, when broken sites are staggered, the load on neighboring unbroken fibers is less than it would be if the breaks had aligned because of this effect.

In their analyses, Sastry and Phoenix[26,27] dealt primarily with the consequences of the nonaligned breaks and not on the factors that caused their occurrence. These researchers did note, however, that the statistical failure of fibrous composites should lead to some nonalignment of fiber breaks, even with the overload profile in adjacent fibers delineated by Hedgepeth and van Dyke.[6]

Research by Grubb and coworkers[11,33] with 2D arrays of Nicalon fibers embedded in a room temperature epoxy resin showed that a decrease in the interfiber spacing increases the mean fragment length and fragment aspect ratio at saturation. From this work, aggregate histograms of fiber-fragment distributions from single- and multi-fiber-fragmentation test data are illustrated in Figure 5. Although the multifiber specimen broke before saturation, the apparent shift in the maximum of this distribution to a higher average fragment length is consistent with the Grubb and coworkers[11,33] test data.

However, a preliminary look at the individual fibers in the multi-fiber-fragmentation specimen revealed that the fragment distributions of the {±2 and 0} fibers were similar, with average fragment lengths of (363 ± 115), (355 ± 129), and (356 ± 91) μm, respectively. The average fragment lengths of the {±1} fibers were similar [(284 ± 90) and (276 ± 93) μm, respectively] but statistically different from the {±2 and 0} fibers,

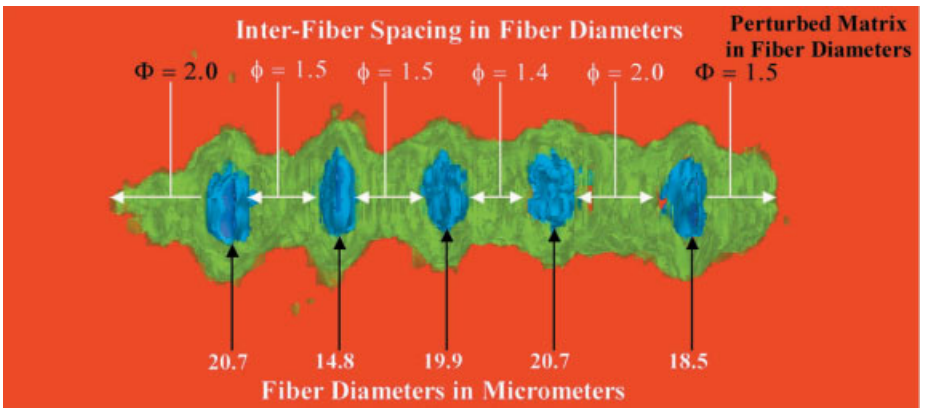

Figure 8. OCT image of a multiple E-glass fibers (blue) embedded in DGEBA/*m*-PDA matrix (red). Green region surrounding the fibers denotes residual curing stresses. Data were obtained with optical coherence tomography.

with a p value at the 95% confidence level of 3.15E-07. Aggregate histograms of this result are displayed in Figure 6. The distribution maximum of the {±1} fibers is similar to the single-fiber-fragmentation test. Therefore, the apparent shift in average fragment length maximum of the multifiber is associated with the {±2 and 0} fibers. The larger average fragment length for the {0} fiber may reflect a more complicated interaction process for these specimens than observed by Grubb and coworkers.[11,33]

Because the DGEBA/*m*-PDA epoxy resin is cured with a two-stage temperature profile, residual cure stresses in the 2D multi-fiber-array model composites may also influence the observed fragmentation patterns and the deformation behavior observed in the matrix. Preliminary optical coherence tomography (OCT) data,[34,35] showing isosurface plots of a single-fiber and 2D multifiber array are presented in Figures 7 and 8. OCT is a noninvasive, noncontact optical imaging technique that allows the visualization of features within scattering media with precise knowledge of the location of these features.

The OCT image data in Figures 7 and 8 were first processed with custom written programs in MATLAB® (Mathworks, Inc.). The sequential, raw binary data were read in and converted to 8-bit grayscale image data. The image color map was inverted and gamma corrected to increase contrast. The image set was then saved in TIF format.

The TIF slices were sequentially read into volumetric visualization software (T3D from Fortner Research) and displayed as false color images. In these figures, the blue color represents highly reflecting features, the green is moderately reflecting features, and the red shows features that reflect very little. The images are depicted with the fibers perpendicular to the plane of the article. In these images, four isointensity color plots are shown—53 (dark blue), 65 (light blue), 161 (green), and 250 (red). The images are representative of the features along the fiber axis.

In Figure 7, an image of the cross section of an unbroken 19 μm glass fiber (blue), as measured by OCT, is shown embedded in DGEBA/*m*-PDA epoxy resin (red). The elongation of the circular fiber in the vertical direction is an unresolved double-reflection artifact caused by the glass fiber acting as a lens. Of importance in this plot is the uniform color of the matrix surrounding the fiber. The resolution of the OCT technique in these plots is approximately 12 μm; therefore, within this resolution the stress in the bulk matrix is not perturbed by the presence of the glass fiber.

In Figure 8, an image plot of the cross section of an unbroken 2D five-fiber array is shown. The fiber diameters measured by OCT are given in micrometers, and the interfiber distance, denoted by Φ, is given as before with 19 μm as the reference diameter. In contrast to Figure 7, there is a region in the multifiber array of a perturbed matrix that surrounds the fibers (shown in green). As in the previous figure, the fibers are shown in blue and the unperturbed matrix is red. The perturbed matrix material beyond the edge of the multifiber array, Φ, is also given in fiber diameters.

Because this perturbed region is absent in the single-fiber specimen, this region seems to be due to residual cure stresses caused by the close proximity of the adjacent embedded fibers and the higher thermal-expansion coefficient of the matrix. This interpretation is based on the observation that OCT images are obtained from light that is backreflected and backscattered from microstructural features within the material.[36,37] In the single-fiber specimen, the matrix shrinks uniformly around the fiber, and the polymer chains are randomly oriented; therefore, the microstructural features are spatially uniform. In the multifiber specimen, this spatial uniformity is destroyed by the close proximity of the fibers and the adhesive bond between the fibers and the matrix. We believe this causes the polymer chains to align between the fibers because the thermal-expansion coefficient of the matrix is higher than the fibers, thereby creating residual curing stresses. This perturbs the chain orientation immediately beyond the fiber radius. Thus, the polymer chains in this region are not randomly oriented and reflect light differently than the bulk matrix.

It appears that matrix cracks influence the interactions between adjacent fibers in a manner different from that described by the present models. Research is ongoing in an attempt to quantify this interaction.

REFERENCES AND NOTES

1. Spragg, C. J.; Drzal, L. T. Fiber, Matrix, and Interface Properties; American Society for Testing and Materials: West Conshohocken, PA, 1996, pp 1–200.
2. Sierakowski, R. L.; Newaz, G. M. Damage Tolerance in Advanced Composites; Technomic: Lancaster, PA, 1995, pp 1–52.
3. Mamalis, A. G.; Manolakos, D. E.; Demosthenous, G. A.; Ioannidis, M. B. Crashworthiness of Composite Thin-Walled Structural Components; Technomic: Lancaster, PA, 1998, pp 1–259.
4. Wagner, H. D.; Steenbakkers, L. W. J Mater Sci 1989, 24, 3956–3975.
5. Phoenix, S. L.; Beyerlein, I. J. Comprehensive Composite Materials. In Fiber Reinforcements and General Theory of Composites; Kelly, A.; Zweben, C., Eds.; Elsevier: Amsterdam, 2000; Vol. 1, Chapter 19, pp 559–639.
6. Hedgepeth, J. M.; van Dyke, P. J Comp Mater 1967, 1, 294–309.
7. van den Heuvel, P. W. J.; Peijs, T.; Young, R. J. J Mater Sci Lett 1996, 15, 1908–1911.
8. van den Heuvel, P. W. J.; Peijs, T.; Young, R. J. Compos Sci Technol 1997, 57, 899–911.

9. van den Heuvel, P. W. J.; Peijs, T.; Young, R. J. Compos Sci Technol 1998, 58, 933–944.
10. van den Heuvel, P. W. J.; Peijs, T.; Young, R. J. Compos A 2000, 31, 165–171.
11. Grubb, D. T.; Li, Z. F.; Phoenix, S. L. Compos Sci Technol 1995, 54, 237–249.
12. Wagner, H. D.; Amer, M. S.; Schadler, L. S. J Mater Sci 1996, 31, 1165–1173.
13. Wagner, H. D.; Amer, M. S.; Schadler, L. S. Appl Compos Mater 2000, 7, 209–217.
14. Amer, M. S.; Schadler, L. S. Sci Eng Compos Mater 1998, 7, 115–149.
15. Amer, M. S.; Schadler, L. S. J Raman Spectrosc 1999, 30, 919–928.
16. Beyerlein, I. J.; Amer, M. S.; Schadler, L. S.; Phoenix, S. L. Sci Eng Compos Mater 1998, 7, 151–204.
17. Schadler, L. S.; Amer, M. S.; Iskandarani, B. Mech Mater 1996, 23, 205–216.
18. Galiotis, C.; Paipetis, A.; Marston, C. J Raman Spectrosc 1999, 30, 899–912.
19. Chohan, V.; Galiotis, C. Compos Sci Technol 1997, 57, 1089–1101.
20. Stanford, J. L.; Lovell, P. A.; Thongpin, C.; Young, R. J. Compos Sci Technol 2000, 60, 361–365.
21. Young, R. J.; Thongpin, C.; Stanford, J. L.; Lovell, P. A. Compos A 2001, 32, 253–269.
22. Wood, J. R.; Zhao, Q.; Frogley, M. D.; Meurs, E. R.; Prins, A. D.; Peijs, T.; Dunstan, D. J.; Wagner, H. D. Phys Rev B 2000, 62, 7571–7575.
23. Zhao, Q.; Frogley, M. D.; Wagner, H. D. Compos Sci Technol 2001, 61, 2139–2143.
24. Frogley, M. D.; Zhao, Q.; Wagner, H. D. Physical Review B 2002, 65, 113413.
25. Zhao, Q.; Frogley, M. D.; Wagner, H. D. Compos Sci Technol 2002, 62, 147–150.
26. Sastry, A. M.; Phoenix, S. L. SAMPE J 1994, 30, 61–67.
27. Sastry, A. M.; Phoenix, S. L. J Mater Sci Lett 1993, 12, 1596–1599.
28. Daniel, I. M.; Ishai, O. Engineering Mechanics of Composite Materials; Oxford University Press: Oxford, 1994, 89.
29. Drzal, L. T.; Herera-Franco, P. J. In Engineered Materials Handbook: Adhesives and Sealants; ASM Int: Metals Park, OH, 1990; pp 391–405.
30. Holmes, G. A.; Feresenbet, E.; Raghavan, D. Proceedings of the 24th Annual Meeting of the Adhesion Society, The Adhesion Society, Blacksburg, VA, 24061–0201, Feb 2001, pp 62–64.
31. Heise, A.; Menzel, H.; Yim, H.; Foster, M. D.; Wieringa, R. H.; Schouten, A. J.; Erb, V.; Stamm, M. Langmuir 1997, 13, 723–728.
32. Anderson, T. L. Fracture Mechanics: Fundamentals and Applications; CRC: Boca Raton, FL, 1991; pp 308–309.
33. Li, Z. F.; Grubb, D. T.; Phoenix, S. L. Compos Sci Technol 1995, 54, 251–266.
34. Dunkers, J. P.; Holmes, G. A.; McDonough, W. G. Proceedings of the 24th Annual Meeting of the Adhesion Society, The Adhesion Society, Blacksburg, VA, 24061–0201, Feb 2001, pp 74–76.
35. Dunkers, J. P.; Phelan, F. R.; Sanders, D. P.; Everett, M. J.; Green, W. H.; Hunston, D. L.; Parnas, R. S. Opt Lasers Eng 2001, 35, 135–147.
36. Huang, D.; Swanson, E. A.; Lin, C. P.; Schuman, J. S.; Stinson, W. G.; Chang, W.; Hee, M. R.; Flotte, T.; Gregory, K.; Puliafito, C. A.; Fujimoto, J. G. Science 1991, 254, 1178–1181.
37. Handbook of Optical Coherence Tomography; Bouma, B. E.; Tearney, G. J., Eds.; Marcel Dekker: New York, 2002, pp 1–40.